Acta Crystallographica Section D
Biological Crystallography
ISSN 0907-4449

Structure of a complex of the potent and specific inhibitor BW284C51 with *Torpedo californica* acetylcholinesterase

Clifford E. Felder,[a] Michal Harel,[a] Israel Silman[b] and Joel L. Sussman[a]*

[a]Department of Structural Biology, Weizmann Institute, Rehovot, Israel, and [b]Department of Neurobiology, Weizmann Institute, Rehovot, Israel

Correspondence e-mail: joel.sussman@weizmann.ac.il

Received 19 February 2002
Accepted 2 July 2002

PDB Reference: acetylcholinesterase–BW284C51 complex, 1e3q, r1e3qsf.

The X-ray crystal structure of *Torpedo californica* acetylcholinesterase (*Tc*AChE) complexed with BW284C51 {CO[$-CH_2CH_2-pC_6H_4-N(CH_3)_2(CH_2-CH{=}CH_2)]_2$} is described and compared with the complexes of two other active-site gorge-spanning inhibitors, decamethonium and E2020. The inhibitor was soaked into *Tc*AChE crystals in the trigonal space group $P3_121$, yielding a complex which diffracted to 2.85 Å resolution. The structure was refined to an R factor of 19.0% and an R_{free} of 23.4%; the final model contains the protein, inhibitor, 132 water molecules and three carbohydrate moieties. BW284C51 binds similarly to decamethonium and E2020, with its two phenyl and quaternary amino end-groups complexed to Trp84 in the catalytic site and to Trp279 in the peripheral binding site, and its central carbonyl group hydrogen bonded very weakly to Tyr121. Possible reasons for decamethonium's weaker binding are considered. The relative strength of binding of bisquaternary inhibitors to acetylcholinesterase and the effect of several mutations of the enzyme are discussed in the context of the respective X-ray structures of their complexes with the enzyme.

1. Introduction

The principal role of acetylcholinesterase (AChE) is termination of impulse transmission at cholinergic synapses by rapid hydrolysis of the neurotransmitter acetylcholine (ACh; Taylor, 1996). In keeping with its biological function, it has an unusually high turnover number, especially for a serine hydrolase (Quinn, 1987). The three-dimensional structure of *Torpedo californica* AChE (*Tc*AChE) revealed that its active site is located at the bottom of a long and narrow cavity lined with aromatic residues, which was named the 'active-site gorge' (Sussman *et al.*, 1991). The active site contains a catalytic triad and an oxyanion hole, similar to those found in other serine hydrolases (Steitz & Shulman, 1982), an acyl pocket which recognizes the acetyl group (Harel *et al.*, 1992) and a so-called 'anionic site', which recognizes the quaternary group of ACh. Surprisingly, the principal component of this anionic site is not a cluster of negative charges, as previously postulated (Nolte *et al.*, 1980), but rather the indole moiety of Trp84, which makes a π–cation interaction (Dougherty & Stauffer, 1990; Felder *et al.*, 2001) with the quaternary group of ACh (Sussman *et al.*, 1991). A second aromatic residue, Phe330, is also involved in recognition of quaternary ligands and, perhaps, also of ACh (Harel *et al.*, 1993).

It has long been known that certain bisquaternary ligands display a much higher affinity for AChE than homologous monoquaternary ligands (Bergmann *et al.*, 1950; Changeux,

1966; Mooser *et al.*, 1972). This led to the definition of a so-called 'peripheral' anionic binding site, with the assumption that the bisquaternary ligands span the two anionic sites. The X-ray structure of the complex of the bisquaternary ligand decamethonium with *Tc*AChE, together with site-directed mutagenesis (Harel *et al.*, 1992, 1993), clearly showed this peripheral site to be located close to the mouth of the active-site gorge. Furthermore, aromatic residues, principally Tyr70 and Trp279, were again shown to be important elements of this so-called 'anionic' site.

Owing to the pharmacological and toxicological importance of AChE, a broad repertoire of ligands selective for it have been developed over the years. Many of these inhibitors are indeed bisquaternary or bistertiary ligands, designed to span the two 'anionic' sites and, as we now know, to span the length of the active-site gorge. These include, apart from decamethonium (DECA), the potent and specific AChE inhibitor, 4-(5-{4-[dimethyl(prop-2-enyl)ammonio]phenyl}-3-oxopentyl)-*N,N*-dimethyl-*N*-prop-2-enylbenzenaminium dibromide, BW284C51, which we abbreviate here as BW (Austin & Berry, 1953) and the very potent series of ambenonium compounds (Hodge *et al.*, 1992; Lands *et al.*, 1958). Bisquaternary oximes, used as antidotes for treatment of nerve-gas intoxication, have also been developed (Ashani *et al.*, 1995; Millard & Broomfield, 1995). More recently, in an effort to develop a new anti-Alzheimer drug selective for AChE, the Eisai Company in Japan adopted a QSAR approach to synthesize and evaluate a large family of *N*-benzylpiperidine-based AChE inhibitors. One of these inhibitors, E2020, under the trade name of Aricept, is now widely used for management of Alzheimer's disease (Kawakami *et al.*, 1996). E2020, although an elongated molecule, is not bisquaternary and so does not bear obvious resemblance to the bifunctional AChE inhibitors mentioned above. Nevertheless, it displays both high affinity and high selectivity for AChE. The solution of the three-dimensional structure of the complex of E2020 with *Tc*AChE revealed a high degree of structural complementarity between the ligand and the enzyme (Kryger *et al.*, 1999).

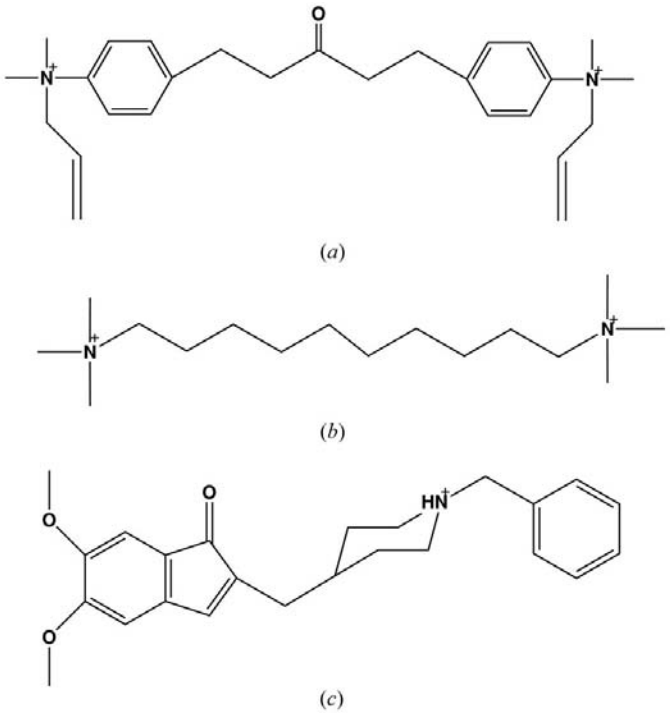

Figure 1
Structures of three gorge-spanning *Tc*AChE inhibitors: (*a*) BW284C51 (BW), (*b*) decamethonium (DECA) and (*c*) E2020.

Table 1
Data-collection and processing.

Values in parentheses refer to the highest resolution shell, 3.16–2.83 Å.

Detector	Xentronics area detector at room temperature
Source	Rigaku FR300 (50 mA, 50 kV)
Wavelength (Å)	1.54184 (Cu $K\alpha$)
Resolution range (Å)	23.0–2.83
No. of measured reflections	36141
No. of unique reflections	22837
Completeness (%)	90.7 (68.4)
$R_{sym}(I)$	0.10 (0.29)
$I/\sigma(I)$	6.9 (2.5)
Space group	Trigonal $P3_121$, #152
Unit-cell parameters (Å, °)	a = 114.0, b = 114.0, c = 138.2, α = 90, β = 90, γ = 120
No. of molecules in unit cell	6

Table 2
Refinement and model statistics.

From *CNS* (Brünger *et al.*, 1998).

Resolution range (Å)	20.0–2.85
No. of reflections	22783
Completeness (%)	92.4
Test set (% of data)	4.5
R factor, R_{free} (%)	19.0, 23.4
No. of atoms	
Non-H protein atoms (533 residues)	4243
Hetero (carbohydrate, BW inhibitor, water, other) atoms	42, 30, 132, 5
R.m.s.d. from ideal values	
Bond lengths (Å)	0.011
Bond angles (°)	1.7
Dihedral angles (°)	23.8
Improper torsion angles (°)	1.06
Estimated coordinate error	
Low-resolution cutoff (Å)	5.00
E.s.d. from Luzzati plot (Å)	0.35
E.s.d. from σ_A (Å)	0.90

It has been known for over 15 y that aromatic residues in proteins interact with other aromatic residues and with aromatic ligands *via* both stacking and herringbone interactions (Burley & Petsko, 1985; Hunter *et al.*, 1991). More recently, the importance of the interaction of aromatic residues with cationic species *via* cation–π interactions has also been realised (Dougherty & Stauffer, 1990; Felder *et al.*, 2001; Gallivan & Dougherty, 1999; Sussman *et al.*, 1991; Verdonk *et al.*, 1993). Although both types of interactions are obviously important for ligand–protein interactions, it has not proved easy to quantify their relative contributions.

In this study, we report the crystal structure of the complex of BW with *Tc*AChE and compare it with the previously determined structures of the DECA–*Tc*AChE (Harel *et al.*,

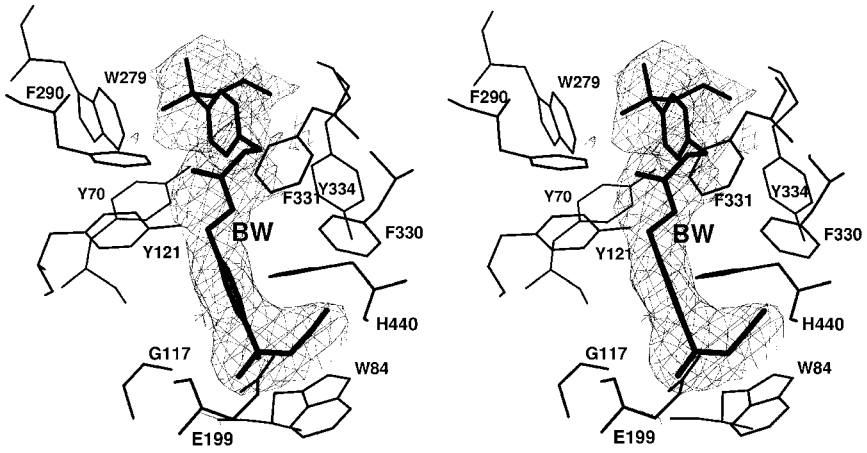

Figure 2
Stereoview of BW in the active site of *Tc*AChE. The BW is shown fitted inside the electron density of a a simulated-annealing $F_o - F_c$ omit map.

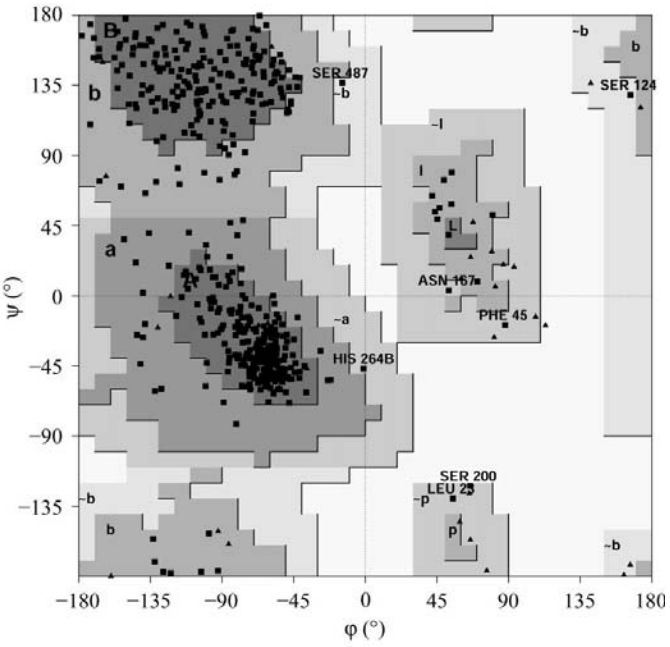

Figure 3
Ramachandran plot of the BW–*Tc*AChE complex, produced with *PROCHECK* (Laskowski *et al.*, 1993).

1993) and E2020–*Tc*AChE (Kryger *et al.*, 1999) complexes (see Tables 1 and 2, and Fig. 1). Since DECA lacks aromatic groups and E2020 has only a single tertiary amino group, BW, which has both an aromatic ring and a quaternary amino group at each extremity plus a carbonyl in the middle that could potentially form a hydrogen bond with a suitable donor, might be expected to bind to AChE more tightly than either DECA or E2020. Indeed, the reported inhibition constant K_i for DECA, in the micromolar range, is about 100 times weaker than that of BW (Cousin *et al.*, 1996; Radic *et al.*, 1993), but that of E2020 is of the same order of magnitude as that of BW (Saxena *et al.*, 2000). By comparison of their respective crystal structures, we hoped to gain a better understanding of the reasons for their different affinities.

2. Methods

2.1. Data collection

Crystals of the complex of BW with *Tc*AChE were obtained by soaking native trigonal crystals of the enzyme (Sussman *et al.*, 1991) in mother liquor [65% saturated $(NH_4)_2SO_4$/0.36 *M* phosphate pH 6.3] containing 2 m*M* BW for one month at room temperature. X-ray data were collected at room temperature to 2.83 Å resolution, as for the native crystals (Sussman *et al.*, 1991), using a Xentronics area detector mounted on an Rigaku RU-300 18 kW rotating-anode generator (see Table 1).

2.2. Refinement

The structure was determined using the difference Fourier technique, based on the native crystal structure of *Tc*AChE (PDB code 1ace; Sussman *et al.*, 1991). This was followed by refinement with *CNS* (Brünger *et al.*, 1998). Subsequently, $F_o - F_c$ and $3F_o - 2F_c$ maps were used to fit the BW molecule, three carbohydrate moieties bonded to Asn59, Asn416 and Asn457, 132 water molecules and one sulfate ion.

The programs *XTALVIEW* (McRee, 1999) and *O* (Jones *et al.*, 1991) were used for model building. The starting model of BW was taken from the structure of (*R*)-2,*trans*-6-diphenyl-*cis*-3-methyl-4-thianone found in the Cambridge Structural Database (CSD) (Ramalingam *et al.*, 1979). The quaternary moieties were taken from the edrophonium–*Tc*AChE complex (PDB code 1ack; Harel *et al.*, 1993). For refinement of BW in the complex, alkane C—C equilibrium bonds were parameterized at 1.52 Å, aromatic bonds at 1.39 Å, alkene bonds at 1.33 Å and C—N bonds at 1.49 Å. The sp^2 bond angles were set to 120° and sp^3 bond angles to 110°. No torsional constraints were assigned to sp^3—sp^2 bonds, to allow only the electron density to determine their conformations. The refinement results are summarized in Table 2. Fig. 2 displays a portion of a simulated-annealing omit $F_o - F_c$ map (Bhat, 1988) based on the final refined coordinates and omitting all non-protein atoms, showing the region in which BW is bound to the enzyme.

The final coordinates were validated by use of *PROCHECK* (Laskowski *et al.*, 1993) and of the WhatCheck option (Hooft *et al.*, 1996) of *WHAT-IF* (Vriend, 1990). A Ramachandran plot (Fig. 3) shows that virtually the entire structure is within allowed regions.

3. Results and discussion

3.1. The BW–*Tc*AChE structure

The overall structure is similar to both 1ace (Sussman *et al.*, 1991) and 2ace (Raves *et al.*, 1997), with a C_α r.m.s. deviation of 0.42 Å relative to the latter. Improvements in refinement

methodology (Brünger *et al.*, 1998) allowed us to trace the backbone chain and some side chains missing in 1ace. Specifically, we were able to extend the N-terminus by one residue (His3), to see the external loop comprising residues 484–490 and to identify three *N*-acetyl-D-glucosamine (NAG) groups attached to Asn59, Asn416 and Asn457. The C-terminus was too disordered to permit fitting of residues beyond Ala534, as was the case for 2ace (Raves *et al.*, 1997), or to fit an NAG residue on the putative glycosylation site at Asn533.

From consideration of the stereoview of BW complexed inside the active-site gorge of *Tc*AChE shown in Fig. 4, together with the *LIGPLOT* diagrams displayed in Fig. 5(*a*), the following assignments can be made for protein–inhibitor interactions. Near the top of the gorge, the distal quaternary group of BW makes a quaternary interaction with Trp279 and a herringbone aromatic interaction with Tyr334. In the middle of the gorge there is a weak hydrogen bond of 3.53 Å between the BW carbonyl and Tyr121 OH, as well as alkyl interactions with Phe331. The distal carbon of the allyl group makes a C—H···O hydrogen bond with Gln74 OE1. At the bottom of the gorge there is an aromatic–aromatic interaction between the proximal phenyl ring of BW and His440 and a cation–aromatic interaction between the proximal quaternary group and Trp84, as well as an electrostatic interaction between the same quaternary group and Glu199. The distal carbon of the allyl group makes a hydrophobic interaction with Phe330.

3.2. Overall comparison of the complexes

The *LIGPLOT* (Wallace *et al.*, 1995) diagrams in Fig. 5 show atom–atom contacts of <3.65 Å made by the three inhibitors, *viz.* BW, DECA and E2020, with amino-acid residues lining the active-site gorge. The inhibitors also make cation–π and π–π interactions with nearby aromatic side-chains (Tyr70, Trp84, Trp279 and Phe330 or Tyr334), as shown in red dashed lines in Fig. 4 for BW (similar interactions occur with the other two inhibitors). These interactions would be expected to make a significant contribution to their overall binding strength.

As can be seen in the stereo superposition of the three inhibitors oriented along the active-site gorge of *Tc*AChE in Fig. 6, DECA and E2020 appear to follow a similar trajectory along the gorge, while BW traces a different route, especially near the anionic site at its bottom. As a result, the phenyl ring of Phe330, which interacts strongly with BW, assumes a quite different conformation. Otherwise, the side-chain conformations are similar for all three complexes.

Table 3
Comparison of wild-type and mutant AChE inhibitor-binding constants for three gorge-spanning AChE inhibitors.

The values in parentheses are the ratios of the mutant to corresponding wild-type K_i values. The values for chicken AChE are compared with the data for *Tc*AChE from Eichler *et al.* (1994).

Enzyme	BW	DECA	E2020
Torpedo WT	2.0 n*M*†; 15, 64 n*M*‡	0.34 µ*M*†; 1.3, 7.0 µ*M*‡	3.1, 4.0 n*M*§
Mouse WT	2.8, 4.8 n*M*¶	3.5, 31 µ*M*¶	2.2, 23 n*M*§
Mouse, Y70N††	24, 29 n*M*¶ (8.6, 6.0)	22, 95 µ*M*¶ (6.3, 3.0)	20, 50 n*M*§ (9.1, 2.2)
Mouse, D72N††	1900, 2300 n*M*¶ (679, 479)	830, 3000 µ*M*¶ (237, 97)	5, 16 µ*M*§ (2272, 696)
Mouse, W84A††	—	—	0.7, 1.4 µ*M*§ (318, 61)
Mouse, Y121Q††	16, 60 n*M*¶ (5.7, 12.5)	26, 68 µ*M*¶ (7.4, 2.2)	20, 50 n*M*§ (9.1, 2.2)
Mouse, W279R††	240, 490 n*M*¶ (86, 102)	390, 1300 µ*M*¶ (111, 42)	—
Mouse, W279A††	—	—	3.2,4.8 µ*M*§ (1455, 209)
Chicken WT	240 n*M*‡‡ (120)	23.6 µ*M*‡‡ (69)	—

† K_i', wild-type *Tc*AChE (Eichler *et al.*, 1994). K_i and K_i' are the equilibrium binding constants of the inhibitor to the free enzyme and to the acyl enzyme, respectively. ‡ K_i, K_i', wild-type *Tc*AChE (Cousin *et al.*, 1996). § K_i, K_i', *Torpedo* wild-type or mouse AChE (Saxena *et al.*, 2000). ¶ K_i, K_i', mouse AChE (Radic *et al.*, 1993). †† All residue numbering is that of *Tc*AChE. ‡‡ K_i' for chicken AChE (Eichler *et al.*, 1994).

3.3. Factors contributing to relative inhibitor-binding strength

As shown in Table 3, the experimental inhibition constants K_i for *Tc*AChE range from 2.0 to 64 n*M* for BW and E2020, but from 0.34 to 7.0 µ*M* for DECA (Eichler *et al.*, 1994; Cousin *et al.*, 1996; Saxena *et al.*, 2000), corresponding to ∼100-fold weaker binding. Several factors determine the relative binding strength of different inhibitors to a given protein binding site, including conformational flexibility of the inhibitor and amino-acid residues in the ligand-binding site, tightness of steric fit, number of favourable (*e.g.* hydrogen bonding, cation–π and π–π interactions, salt bridges and other electrostatic or electronic

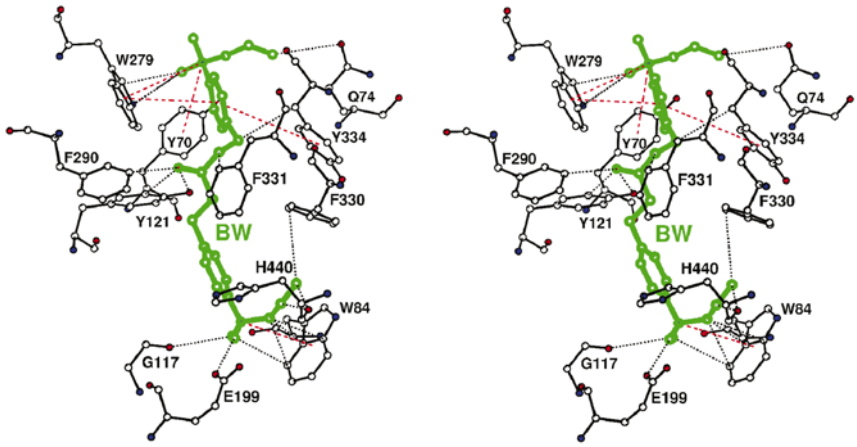

Figure 4
Stereoview of BW in the active site of *Tc*AChE, including the closest residues with which it makes contact (black dashed lines) and the principal quaternary amine–aromatic and aromatic–aromatic interactions (red dashed lines).

interactions) compared with unfavorable interactions (*e.g.* steric hindrance), desolvation of the inhibitor and the complexed binding site residues and involvement of solvent molecules in binding. Factors favouring the tighter binding of BW and E2020 over DECA include their both being conformationally less flexible (E2020 is even less flexible than BW), their aromatic groups (which DECA lacks) making favourable π–π interactions with nearby aromatic residues in addition to cation–π interactions with their quaternary amino groups, and their greater bulk (especially of that of E2020), which produces a tighter fit inside the binding site. The role of water molecules is more difficult to assess, since the resolutions of the BW and DECA crystal structures were too low to permit identification of crystallographic waters inside the active-site gorge (Koellner *et al.*, 2000). In the case of E2020, however, the role of water molecules in bonding has been demonstrated (Kryger *et al.*, 1999).

3.4. Effects of mutations of AChE on K_i values

Measured K_i values for mutant AChEs, as shown in Table 3, can provide independent evidence that the residues shown in Fig. 5 are involved in favourable contacts. Although there are no data for *Tc*AChE mutants, the measured K_i values for the mouse wild-type enzyme, 2.8–4.8 n*M*, 3.5–31 µ*M* (Radic *et al.*, 1993) and 2.2–23 n*M* (Saxena *et al.*, 2000), for BW, DECA and E2020, respectively, are similar to the corresponding values for the *Torpedo* enzyme. However, those for some of the mutants differ by orders of magnitude. Hence, we can make use of K_i values for mouse AChE together with structural data for *Tc*AChE when discussing the key residues involved in binding. For the mouse Trp279→Arg mutant (all residue numbering refers to *Tc*AChE), the measured K_i values increase about 100-fold to 240–490 n*M* and 390–1300 µ*M* for BW and DECA,

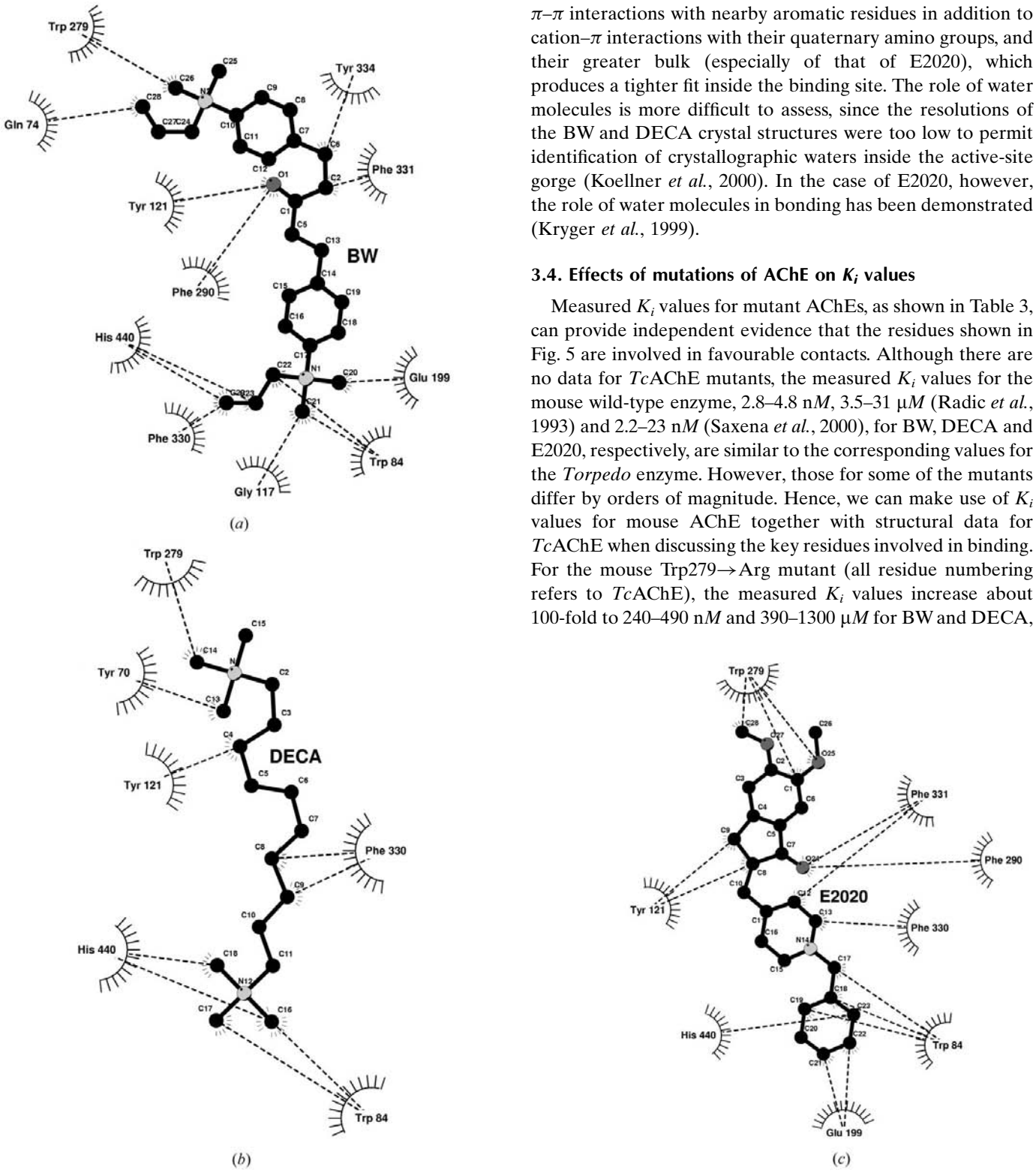

Figure 5
Schematic diagrams using *LIGPLOT* (Wallace *et al.*, 1995), of the closest atom–atom contacts (<3.65 Å) made by (*a*) BW, (*b*) DECA and (*c*) E2020 with adjacent residues (excluding waters) inside the active-site gorge of TcAChE. The differences in the contacts between the three inhibitors are related to the alternate routes that they trace along the gorge and to differences in their flexibility and bulkiness.

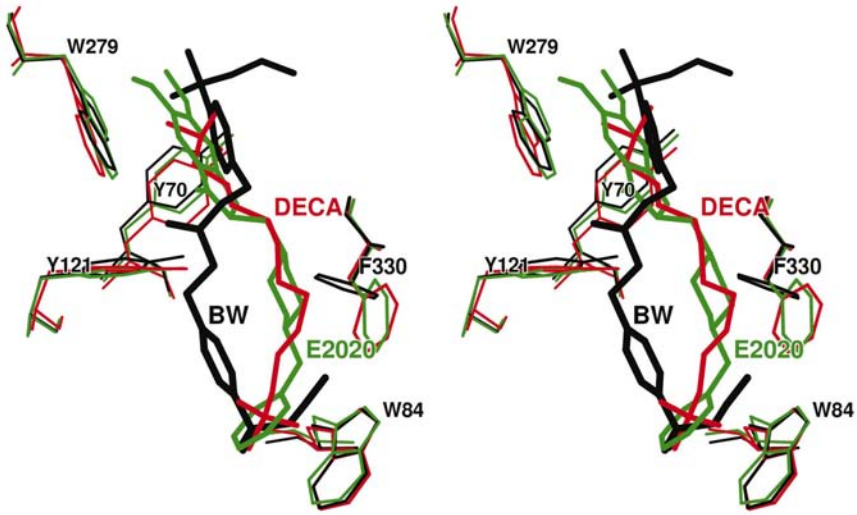

Figure 6
Stereoview of a superposition of BW, DECA and E2020 within the active-site gorge of *Tc*AChE. The BW itself and key amino-acid residues are displayed in black, DECA and the corresponding amino-acid residues are displayed in red and E2020 and the corresponding amino-acid residues are displayed in green.

respectively, and Trp279→Ala causes an increase *ca* 1000-fold to 3.2–4.8 μ*M* for E2020. For the Trp84→Ala mutant, K_i increases ∼500-fold to 0.7–1.4 μ*M* for E2020 (with no corresponding data for BW and DECA being available). These data are consistent with the two Trp residues, Trp84 and Trp279, making the strongest contacts with the inhibitors (Fig. 5). In contrast, with respect to residues that make fewer and weaker contacts, the K_i values for the Tyr70→Gln mutant are 24–29 n*M*, 22–95 μ*M* and 20–50 n*M*, respectively, and for the Tyr121→Asn mutant they are 16–60 n*M*, 26–68 μ*M* and 20–50 n*M*, respectively, increases of less than tenfold in both cases. Finally, chicken AChE, which lacks both Tyr70 and Trp279, can be regarded as a 'natural' mutant compared with *Tc*AChE. Indeed, the K_i values measured for BW and DECA of 240 n*M* and 23.6 μ*M*, respectively, for the chicken enzyme (Eichler *et al.*, 1994) are about ∼100 times weaker than for that of *Tc*AChE, consistent with the mouse AChE data.

There is one mutation, Asp72→Asn, that has a large effect on all the K_i values, although Asp72 does not make close contact with any of the three inhibitors. This residue, which is located close to the peripheral binding site, was found to set up an electrostatic trap which constrains cationic ligands to bind initially to the peripheral site and then to move along a one-dimensional trajectory down a negative electrostatic potential gradient (Felder *et al.*, 1997). In contrast, binding of neutral ligands remains diffusion-controlled until they reach the active site at the base of the gorge (Botti *et al.*, 1999; Radic *et al.*, 1997). Elimination of this trap results in a significant reduction of the kinetic on-rate relative to the off-rate for cationic ligands, resulting in the observed effect on the experimental K_i values, since K_i is the ratio of these two kinetic constants. These data for the Asp72→Asn mutation, taken in conjunction with the structural data, show that caution must be exercised in assessing the effects of site-directed mutagenesis for systems for which structural data are lacking.

This work was supported by the US Army Medical Research Acquisition Activity under Contract No. DAMD17-97-2-7022, the European Union Fifth Framework in Biotechnology, the Kimmelman Center for Biomolecular Structure and Assembly, Rehovot, Israel. IS is Bernstein–Mason Professor of Neurochemistry. The authors thank Professor Felix Frolow and Dr Gideon Schreiber for valuable discussions.

References

Ashani, Y., Radic, Z., Tsigelny, I., Vellom, D. C., Pickering, N. A., Quinn, D. M., Doctor, B. P. & Taylor, P. (1995). *J. Biol. Chem.* **270**, 6370–6380.
Austin, L. & Berry, W. K. (1953). *Biochem. J.* **54**, 695–700.
Bergmann, F., Wilson, I. B. & Nachmansohn, D. (1950). *Biochim. Biophys. Acta*, **6**, 217–224.
Bhat, T. N. (1988). *J. Appl. Cryst.* **21**, 279–281.
Botti, S. A., Felder, C., Lifson, S., Sussman, J. L. & Silman, I. (1999). *Biophys. J.* **77**, 2430–2450.
Brünger, A. T., Adams, P. D., Clore, G. M., DeLano, W. L., Gros, P., Grosse-Kunstleve, R. W., Jiang, J. S., Kuszewski, J., Nilges, M., Pannu, N. S., Read, R. J., Rice, L. M., Simonson, T. & Warren, G. L. (1998). *Acta Cryst.* D**54**, 905–921.
Burley, S. K. & Petsko, G. A. (1985). *Science*, **229**, 23–28.
Changeux, J.-P. (1966). *Mol. Pharmacol.* **2**, 369–392.
Cousin, X., Bon, S., Duval, N., Massoulié, J. & Bon, C. (1996). *J. Biol. Chem.* **271**, 15099–15108.
Dougherty, D. A. & Stauffer, D. A. (1990). *Science*, **250**, 1558–1560.
Eichler, J., Anselmet, A., Sussman, J. L., Massoulié, J. & Silman, I. (1994). *Mol. Pharmacol.* **45**, 335–340.
Felder, C. E., Botti, S. A., Lifson, S., Silman, I. & Sussman, J. L. (1997). *J. Mol. Graph.* **15**, 318–327.
Felder, C., Jiang, H.-L., Zhu, W.-L., Chen, K.-X., Silman, I., Botti, S. A. & Sussman, J. L. (2001). *J. Phys. Chem. A*, **105**, 1326–1333.
Gallivan, J. P. & Dougherty, D. A. (1999). *Proc. Natl Acad. Sci. USA*, **96**, 9459–9464.
Harel, M., Schalk, I., Ehret-Sabatier, L., Bouet, F., Goeldner, M., Hirth, C., Axelsen, P., Silman, I. & Sussman, J. L. (1993). *Proc. Natl Acad. Sci. USA*, **90**, 9031–9035.
Harel, M., Sussman, J. L., Krejci, E., Bon, S., Chanal, P., Massoulié, J. & Silman, I. (1992). *Proc. Natl Acad. Sci. USA*, **89**, 10827–10831.
Hodge, A. S., Humphrey, D. R. & Rosenberry, T. L. (1992). *Mol. Pharmacol.* **41**, 937–942.
Hooft, R. W., Sander, C. & Vriend, G. (1996). *J. Appl. Cryst.* **29**, 714–716.
Hunter, C. A., Singh, J. & Thornton, J. M. (1991). *J. Mol. Biol.* **218**, 837–846.
Jones, T. A., Zou, J.-Y., Cowan, S. W. & Kjeldgaard, M. (1991). *Acta Cryst.* A**47**, 110–119.
Kawakami, Y., Inoue, A., Kawai, T., Wakita, M., Sugimoto, H. & Hopfinger, A. J. (1996). *Bioorg. Med. Chem. Lett.* **4**, 1429–1446.
Koellner, G., Kryger, G., Millard, C. B., Silman, I., Sussman, J. L. & Steiner, T. (2000). *J. Mol. Biol.* **296**, 713–735.

Kryger, G., Silman, I. & Sussman, J. L. (1999). *Structure*, **7**, 297–307.
Lands, A. M., Hoppe, J. O., Arnold, A. & Kirchner, F. K. (1958). *J. Pharmacol. Exp. Ther.* **123**, 121–127.
Laskowski, R. A., MacArthur, M. W., Moss, D. & Thornton, J. M. (1993). *J. Appl. Cryst.* **26**, 283–291.
McRee, D. E. (1999). *J. Struct. Biol.* **125**, 156–165.
Millard, C. B. & Broomfield, C. A. (1995). *J. Neurochem.* **64**, 1909–1918.
Mooser, G., Schulman, H. & Sigman, D. S. (1972). *Biochemistry*, **11**, 1595–1602.
Nolte, H.-J., Rosenberry, T. L. & Neumann, E. (1980). *Biochemistry*, **19**, 3705–3711.
Quinn, D. M. (1987). *Chem. Rev.* **87**, 955–975.
Radic, Z., Pickering, N. A., Vellom, D. C., Camp, S. & Taylor, P. (1993). *Biochemistry*, **32**, 12074–12084.
Radic, Z., Kirchoff, P. D., Quinn, D. M., McCammon, J. A. & Taylor, P. (1997). *J. Biol. Chem.* **272**, 23265–23277.
Ramalingam, K., Berlin, K. D., Loghry, R. A., van der Helm, D. & Satyamurthy, N. (1979). *J. Org. Chem.* **44**, 477–486.
Raves, M. L., Harel, M., Pang, Y.-P., Silman, I., Kozikowski, A. P. & Sussman, J. L. (1997). *Nature Struct. Biol.* **4**, 57–63.
Saxena, A., Fedorko, J. M., Medhekar, R., Taylor, P., Lockridge, O. & Doctor, B. P. (2000). *Proceedings of the USAMRICD 2000 Medical Defense Bioscience Review 2000*, pp. 217–226.
Steitz, T. A. & Shulman, R. G. (1982). *Annu. Rev. Biophys. Bioeng.* **11**, 419–444.
Sussman, J. L., Harel, M., Frolow, F., Oefner, C., Goldman, A., Toker, L. & Silman, I. (1991). *Science*, **253**, 872–879.
Taylor, P. (1996). *The Pharmacological Basis of Therapeutics*, 9th ed., edited by J. G. Hardman, L. E. Limbird, P. B. Molinoff, R. W. Ruddon and A. G. Gilman, pp. 161–176. New York: McGraw–Hill.
Verdonk, M. L., Boks, G. J., Kooijman, H., Kanters, J. A. & Kroon, J. (1993). *J. Comput.-Aided Mol. Des.* **7**, 173–182.
Vriend, G. (1990). *J. Mol. Graph.* **8**, 52–56.
Wallace, A. C., Laskowski, R. A. & Thornton, J. M. (1995). *Protein Eng.* **8**, 127–134.